<Advanced Energy Conversion Division> Clean Energy Conversion Research Section

AUTHOR(S):

Inagaki, Shigeru; Konabe, Satoru

Clean Energy Conversion Research Section

Shigeru Inagaki, Visiting Professor
(Kyushu University)

1. Aim of research

In Heliotron-J, a large amount of time series data has been obtained by the progress of simultaneous multi-point plasma measurements for many years. It is necessary to coarse-grain and visualize this large amount of data to extract deep correlation and hidden causarity. In order to coarse-grain the data under the assumption that "physics is simple", it is necessary to define some kind of simplified model and to quantify and minimize the statistical distance between the observation and the model [1]. Following this approach, we focus on time series data in particular, and extract some temporal patterns inherent in the data. This method can represent the non-stationarity, intermittence, and non-linearity of the plasma with fewer degrees of freedom than the Fourier analysis, which has been the main tool for time series data analysis so far. In this study, we develop such a new analysis tool using Heliotron-J time series data, and discuss the non-stationarity, suddenness, and non-linearity of Heliotron-J plasma. Heliotron-J has accumulated a large amount of time series data as described above, and in addition, it has large-scale data such as digital ECE using ultrafast oscilloscopes, which has been conducted in previous collaborative research. There are few projects in Japan where such data sets are available. Therefore, it is necessary to conduct this project as a collaborative research at Heliotron J.

2. Application of ARMA model to turbulent time series data

In this study, we develop a method for extracting characteristic patterns from time series data. We are not interested in patterns that appear on very short time-scales, but rather those that have relatively long time-scales. For this reason, we consider extracting the longest time-scale from the time series data. However, it is difficult to determine the time scale with high accuracy because the peaks of periodogram of time series data with weak periodicity, such as turbulent flow, are wide. Therefore, we adopted one of the statistical modeling of time series, the ARMA (autoregressive moving average model) [2], which is a model to predict the current value from past time series data and can be written as follows,

$$X(t) = \epsilon(t) + \sum_{i=1}^{p} \varphi_i X(t-i) + \sum_{i=1}^{q} \theta_i \epsilon(t-i),$$

where $X(t)$ is the discrete time series data, $\epsilon(t)$ is the Gaussian noise, φ_i and θ_i are the coefficients, and p and q are the maximum degrees of freedom of the model. In order to obtain the long-term time scale from this model, the maximum degree of freedom of the model becomes large and the computational cost increases accordingly. In this study, we tested how long time-scales can be extracted from the ARMA model by using turbulent time series data obtained from the fundamental plasma experiment. The target time series data are shown in Fig. 1. The ARMA model is a stationary model, so it is applied to the stationary part of the data, which is indicated by the red line in the figure. The extended Dickey-Feller test rejects the non-stationarity of the data with a probability of 1-2 $\times$ 10^{-9} [3]. To reduce the computational cost, a Bessel-type anti-aliasing filter is applied and the sampling frequency is set to 1/20 (50 kHz).

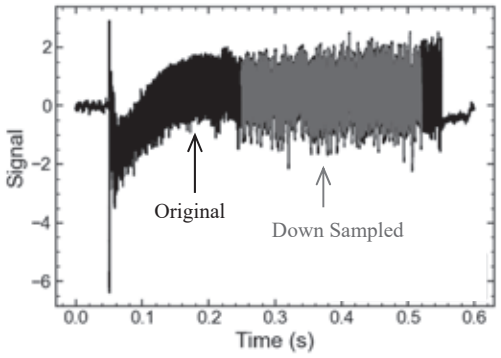

Fig.1: Target time series data. Red line indicates down-sampled data.

3. Detecting long time-scale with the ARMA model

Although there is no general method to determine p and q in the ARMA model, information about p can be obtained from the partial correlation function. The cross-correlation function and the partial cross-correlation function are shown in Fig. 2. The partial correlation function has significantly large values for the first 10 lags. For this reason, 27 models were obtained in a brute force fashion with $1 \le p \le 10$, $0 \le q \le 2$, and the difference from the predicted values was calculated. The best model was determined as the condition that minimizes the Akaike's information criterion [4], and (p, q) = (9, 2) was obtained. The best model is given as $X(t) =$ 0.603+3.30 $X(t-1)$-5.47 $X(t-2)$+ 6.08 $X(t-3)$ - 5.16 $X(t-4)$ + 3.69 $X(t-5)$ - 2.33 $X(t-$

6) + 1.27 $X(t-7)$ - 0.563 $X(t-8)$ + 0.156 $X(t-9)$ - 1.06$\epsilon(t-1)$ + 0.613$\epsilon(t-2)$.

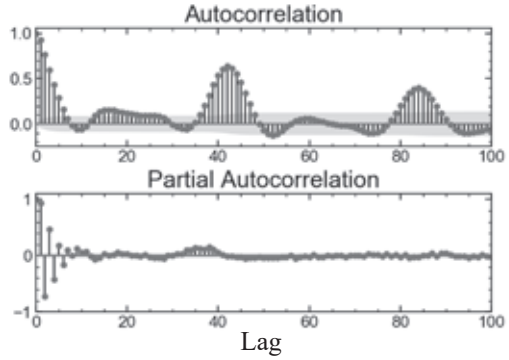

Fig.2: Auto correlation function and partial auto correlation function.

The in-sample prediction (fitting) is shown in Fig. 3. Here initial 2000 points are used as training data. For the in-sample prediction, the ARMA model shows a good agreement. The longest lag obtained is 9×50=450 μs. Although evidence of the in-sample predictability is found, the model shows very poor prediction accuracy for the out-of-sample prediction as shown in Fig. 4.

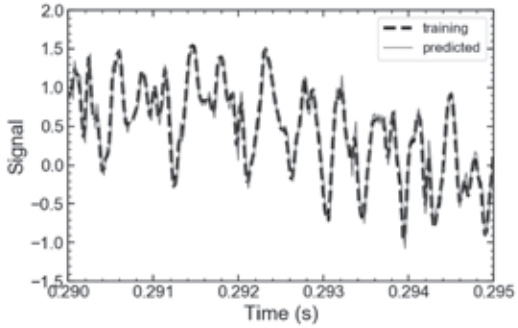

Fig.3: Result of the in-sample prediction.

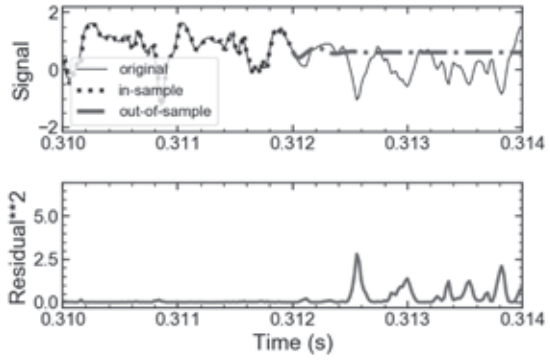

Fig.4: Result of the out-sample prediction and squared residual between model and data.

Why does the ARMA model have poor predictive performance? Figure 5 compares the Fourier spectrum estimated by the ARMA model with the Fourier spectrum of the training data. It can be seen that the ARMA model cannot reproduce the low frequency components. To detect longer periods, we need to explore a larger (p,q) space, which is difficult with the current computational resources. The good predictable capability of the ARMA model does not guarantee the out-of-sample predictability. In order to detect long time-scales at the sacrifice of short time-scales, it is necessary to introduce sparsity into the ARMA model so that the computational cost does not increase even for large (p,q) spaces.

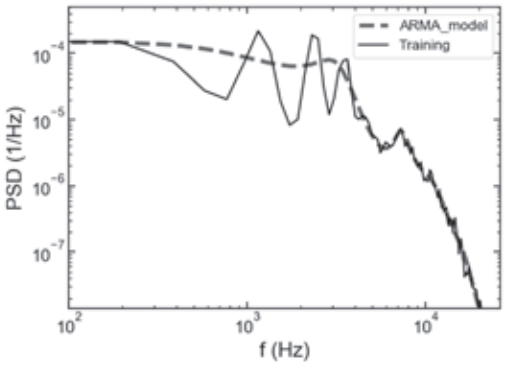

Fig.5: Comparison of the Fourier power spectrum.

4. Discussion and Summary

The performance improvement of out-of-sample prediction for turbulent flow data can be greatly improved by applying deep learning with RNN (Recurrent Neural Network) instead of the ARMA model [5]. However, the RNN is not able to extract the time scale. On the other hand, the ARMA model is good in terms of mapping to physical mechanics, and it can be easily extended to multi-channel data. In the future, we aim to improve the prediction performance by increasing the number of channels to be analyzed and increasing the input information.

References

[1] A. Kusaba, et al., Plasma Fusion Res. 15 (2020) 1301001.
[2] G. E. P. Box, G. M. Jenkins, G. C. Reinsel and G. M. Ljung, Time Series Analysis: Forecasting and Control, 5th Edition, John Wiley and Sons Inc., Hoboken, New Jersey (2015).
[3] J. G. MacKinnon, Journal of Business and Economic Statistics 12 (1994) 167.
[4] H. Akaike, Proceedings of the 2nd International Symposium on Information Theory, Budapest (1973) 267.
[5] T. Mikolov, et. al, Recurrent neural network based language model, Proc. INTERSPEECH 2010.

Clean Energy Conversion Research Section

Satoru Konabe, Visiting Associate Professor
(Hosei University)

1. Introduction

For conventional photovoltaic solar cells, a PN junction is essential for generating a photocurrent via the dissociation of photo-generated electron-hole pairs. However, there is a maximum theoretical power conversion efficiency of PN photovoltaic solar cells, known as the Shockley-Queisser (SQ) limit [1]. A PN junction is not strictly required for photocurrent generation, and an alternative mechanism called the bulk photovoltaic effect (BPVE) [2] has been known. The BPVE generates a steady photocurrent in single-phase homogeneous materials without inversion symmetry. In contrast to the PN photovoltaic effect, the BPVE can generate a photo-voltage above the band gap [3], which makes it possible to overcome the SQ limit [4]and thus surpass the conversion efficiency of conventional solar cells. A primary mechanism in the BPVE is the shift current effect [5,6], a nonlinear optical response where the center of mass of the electron wave function changes in the intracell during photo-excitation [5,7]. First-principles calculations of the shift current have reproduced experimental observations of the BPVE in ferroelectric $BaTiO_3$ [6]. The topological aspects of the shift current have been previously studied [7], and the relation between the shift current and the polarization has been clarified. For a deeper understanding of the BPVE, it is crucial to elucidate the mechanisms that determine the magnitude and direction of the shift current. Recent studies on topological materials found that topologically nontrivial electronic structures give rise to a large shift current response [8]. On the other hand, many-body effects are also important factors that determine the magnitude of the shift current. Morimoto and Nagaosa [9] studied nonlinear excitonic processes and found that the dc current flow is caused by excitons below the band gap without the dissociation of excitons into free electrons and holes. First-principles calculations using the GW and Bethe-Salpeter equation [10] and the time-dependent GW approximation [11] have been conducted to investigate quasiparticle and exciton effects on the shift current. The former demonstrated that excitons reduce the shift current in bulk $BaTiO_3$, but have little influence on the shift current in monolayer SnSe. The latter found that excitons enhance the shift current in monolayer GeS. Importantly, many-body effects become quite noticeable in the optical response, especially that of one-dimensional materials, because almost all the optical intensity is transferred to the lowest exciton state [12,13]. They are thus anticipated to have a crucial influence on the shift current. A recent experiment demonstrated that quasi-one-dimensional transition-metal dichalcogenide nanotubes exhibit an extraordinarily large shift current [14]. However, the exciton effect on the shift current in such one-dimensional materials is still unclear. In the present study, we aim to clarify properties of the shift current in single-walled boron-nitride nanotubes (SW-BNNTs) as a representative one-dimensional material with broken inversion symmetry [15].

2. Shift Current

The shift current is generated to second order in an electric field. For a monochromatic electric field $E_b(t) = E_b(\omega)e^{i\omega t} + E_b(-\omega)e^{-i\omega t}$, the shift current is generally expressed by a response function σ_{sc}^{abc}.

$$J^a = 2\sum_{bc} \sigma_{sc}^{abc}(0,\omega,-\omega)E_b(\omega)E_c(\omega)$$

For the one-dimensional structure considered in the present study, we only consider the component σ_{sc}^{zzz}, where the nanotube axis is parallel to the z direction. Below, we denote σ_{sc}^{zzz} as σ_{sc} for simplicity. By using the equation of motion for the density matrix, the expression for the shift current response function that includes the exciton effect can be obtained as

$$\sigma_{sc}(\omega) = \frac{\hbar e^3}{8\pi V}\sum_{mn}\sum_{kk'k''} \frac{v_{vc,k}v_{cv,k''}^*}{E_m E_n(E_n-\hbar\omega)} \times \psi_k^m \psi_{k'}^{m*}\psi_{k'}^n \psi_{k''}^{n\ *}\left(-\frac{d\log\psi_k^n}{dk'} + i\Omega_{cv,k'}\right) \quad (1)$$

where ψ_k^m is the wave function of nth exciton state at the wavevector of k, E_n is the nth exciton energy, V is the volume of a SW-BNNT, $v_{vc,k}$ is the matrix element between the conduction and valence bands of the velocity operator v, and $\Omega_{cv,k} \equiv \Omega_{cc,k} - \Omega_{vv,k}$, with $\Omega_{mn,k}$ being the Berry connection.

3. Results and Discussion

Figure 1 plots the response function for the shift current calculated using Eq. (1) for the chirality of (10,0) and (11,0) SW-BNNTs. Here, the chiral index (n_1, n_2) uniquely determines the structure of SW-BNNTs. We set the amount of broadening to 0.02 eV. The shift current response in the presence of the exciton effect exhibits symmetric peaks. A comparison with the absorption spectrum indicates that each peak corresponds to the exciton states. For the non-interacting case, the shift current response shows a single asymmetric peak structure starting at the energy of the band gap. A key factor that determines the intensity of the shift current response is the joint density of states (JDOS). For one-

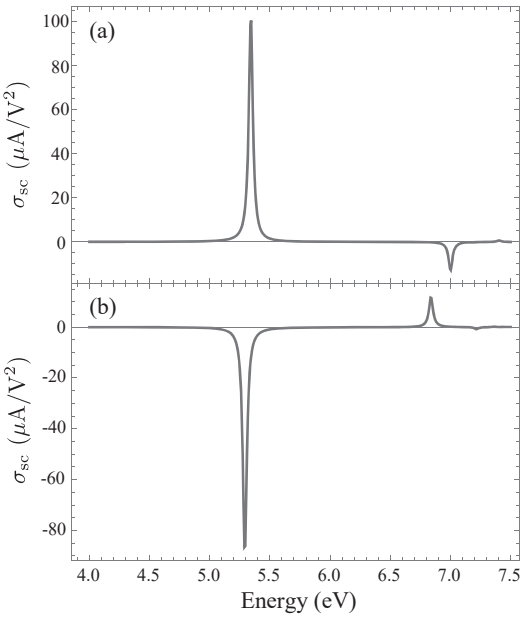

Fig.1 Shift current response for (a) (10,0) and (b) (11,0) SW-BNNT.

dimensional materials like SW- BNNTs, the JDOS is divergently large around the band edge because of the van Hove singularity. In fact, the absorption spectrum becomes largest at the band edge. When the Coulomb interaction effect is included, however, almost all the oscillator strength, which is the largest at the van Hove singularity with the divergently large JDOS for the free electron-hole pairs, is transferred to the lowest exciton state due to exciton formation in one-dimensional materials. As a result, the response of the exciton shift current in a nanotube structure is larger than that of the normal shift current without the exciton effect.

It is important to note that, in Fig. 1, the sign of the response function between (10,0) and (11,0) is opposite for responses with and without the exciton effect. This feature indicates that the direction of the shift current depends on the chiral index of SW-BNNTs. To elucidate the chiral index dependence of the direction of the shift current in SW-BNNTs, we derive an approximate analytical expression for σ_{sc}. Under the assumption that $v_{cv,k}$ is independent of k, Eq. (1) becomes

$$\sigma_{sc} \cong i\frac{e^3\gamma^2 A}{4\pi^3\hbar V}\frac{\Delta}{\kappa_\nu\sqrt{\Delta^2+\gamma^2\kappa_\nu^2}}\sum_n \frac{|\psi^n(z=0)|^2}{E_n^2(E_n-\hbar\omega)} \quad (2)$$

where we have used the relation $\psi^n(z=0) = \frac{1}{\sqrt{A}}\sum_k \psi_k^n$. Because the excitons in SW-BNNTs are Frenkel-type, as determined from ab initio calculations, Eq. (2), whose derivation is justified for Wannier-type excitons where electron and hole pairs are well limited in momentum space to a small neighborhood of $k = 0$, is not expected to quantitatively reproduce the numerical results. However, we can discuss some qualitative features of the exciton shift current in SW-BNNTs. Equation (2) is an odd function of $\kappa_\nu = -2\pi\nu/3L$, where $\nu = \mathrm{mod}(n_1 - n_2, 3)$, and onsite potential Δ, and thus explicitly shows that the sign of the response function is determined by ν and Δ. The sign of the onsite potential is fixed such that $\Delta > 0$ for the B site and $\Delta < 0$ for the N site. We thus conclude that the direction of the exciton shift current is solely determined by ν of SW-BNNTs; the sign of the shift current is positive for (10,0) SW-BNNTs because $\nu = 1(> 0)$, and negative for (11,0) SW-BNNTs because $\nu = -1(< 0)$. Since the parameter ν is defined by the chiral index, the sign of the shift current is determined by the chiral index of SW-BNNTs.

5. Summary

We investigated the exciton effect on the shift current in SW-BNNTs and found that the shift current is enhanced by the exciton effect and that the direction of the shift current is determined by the nanotube chiral index. The present study clarifies remarkable many-body effects in the bulk photovoltaic effect and provides an essential theoretical basis for the control of the shift currents, which will be an important and useful knowledge for future photovoltaic applications.

References

[1] W. Shockley and H. J. Queisser, J. Appl. Phys. 32 510 (1961).
[2] W. Kraut and R. von Baltz, Phys. Rev. B 19 1548 (1979).
[3] W. Ji, K. Yao and Y. C. Liang, Adv. Mater. 22 1763 (2010).
[4] J. E. Spanier et al., Nat. Photon 10, 611(2016).
[5] J. E. Sipe and A. I. Shkrebtii, Phys. Rev. B 61, 5337 (2000).
[6] S. M. Young and A. M. Rappe, Phys. Rev. Lett. 109, 116601 (2012).
[7] T. Morimoto and N. Nagaosa, Sci. Adv. 2, e1501524 (2016).
[8] J. Ma, et. al. Nat. Mater. 18, 476 (2019).
[9] T. Moromoto and N. Nagaosa, Phys. Rev. B 94, 035117 (2016).
[10] R. Fei et. al., Phys. Rev. B 101, 045104 (2020).
[11] Y. H. Chan, et. al., arXiv:1904.12813 (2019).
[12] T. Ogawa and T. Takagahara, Phys. Rev. B 44, 8138 (1991).
[13] T. Ando, J. Phys. Soc. Jpn. 66, 1066 (1997).
[14] Y. J. Zhang, et. al., Nature 570, 349 (2019).
[15] S. Konabe, Phys. Rev. B 103, 075402 (2020).